

QCD at the HERAscale and implications at the Terascale

Achim Geiser
DESY, D-22603 Hamburg, Germany
E-mail: Achim.Geiser@desy.de

1 Introduction

The HERA data of ep collisions at $\sqrt{s} = 318$ GeV currently offer one of the best opportunities to test and improve our understanding of the theory of Quantum Chromodynamics (QCD). HERA data taking has ended in 2007, but most of the results using the full HERA statistics are still in preparation, and will continue to provide new and improved results.

QCD can be probed in high energy electron proton collisions in several different ways. The study of the structure of the proton yields direct measurements of the parton density functions at high energies. Jet measurements (also covered in a separate contribution [1]) yield complementary insights into higher order QCD corrections, and both taken together allow the (experimentally) most precise determinations of the strong coupling constant, α_s . The study of semi-inclusive final states like heavy flavour production and diffraction yield further complementary information about both perturbative and non-perturbative QCD. Most of the measurements obtained at HERA (at the “HERAscale”) have direct consequences in the context of current and future measurements at the Tevatron and at the LHC (at the Terascale). The goal of this contribution is to highlight some of the most important of these measurements, and their implications at the Terascale.

2 Proton structure

Understanding the structure of the proton in terms of its gluon and quark constituents has a threefold physics interest:

- to understand the properties of the proton in its own right.
- to understand the details of the underlying theory of QCD.
- to provide a detailed description of this structure in terms of parton densities, which are an essential input to the physics at hadron colliders such as the Tevatron and the LHC.

2.1 Kinematics of Deep Inelastic Scattering

The most powerful tool to study the structure of the proton is the so-called Deep Inelastic Scattering (DIS) process, in which a high energy lepton is scattered off a proton with large momentum transfer, exchanging a photon (Fig. 1) or a weak vector boson. In many cases, a measurement of the scattered lepton (e.g. electron) is sufficient to obtain access to the most relevant kinematic variables. These include

- The photon/boson virtuality $Q^2 = -q^2$, where $q = l' - l$, and l, l' are the incoming and outgoing lepton four-momenta. For $Q^2 > m_p^2 \sim 1 \text{ GeV}^2$ details of the proton structure can be resolved, and the resolving power increases with increasing Q^2 .
- The Bjorken scaling variable $x = \frac{Q^2}{2Pq}$, where P is the four-momentum of the incoming or target proton. In the case where the scattering is interpreted to occur off a single light quark (parton) inside the proton (quark-parton model process, QPM, Fig. 1), x measures the fraction of the proton momentum carried by this parton.
- The inelasticity $y = \frac{qP}{lP}$, which is a direct measure of the fraction of the lepton momentum transferred to the exchanged boson. In contrast to x , this variable remains meaningful even in the limit $Q^2 < 1 \text{ GeV}^2$ (quasi-real photon), called photoproduction.

The variables Q^2 , x , and y are not independent, and any set of two of them is sufficient to fully describe the lepton part of the scattering. They can be converted into each other via the relation $Q^2 = xys$, where \sqrt{s} is the center-of-mass energy of the lepton-proton system.

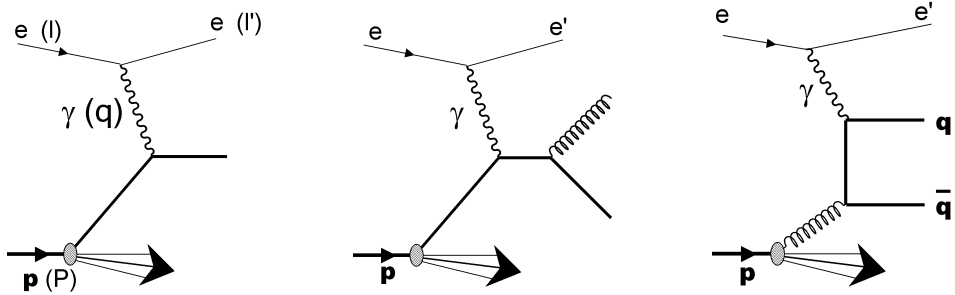


Figure 1: Kinematics of ep scattering for the leading Quark Parton Model process with photon exchange (QPM, left) and graphs for first order QCD corrections: the QCD Compton process (center) and boson gluon fusion (BGF, right).

2.2 Structure Functions and Parton Densities

The double differential cross section as a function of x and Q^2 for the scattering of charged leptons (charge ± 1) off a proton can be parametrized in terms of so-called proton structure functions F_2 , F_L , and xF_3

$$\frac{d^2\sigma}{dx dQ^2} = \frac{2\pi\alpha^2}{Q^4 x} \left\{ [1 + (1-y)^2]F_2(x, Q^2) - y^2 F_L(x, Q^2) \mp [1 - (1-y)^2]xF_3(x, Q^2) \right\}$$

In most general terms, this is nothing but a breakdown of the cross section into a complete set of terms with different y -dependence. It is motivated by the possibility to identify these terms with different physics contributions.

For instance, considering only the simple QPM (0th order QCD) graph of Fig. 1, the structure function F_2 can be understood as a direct measurement of the quark plus antiquark content of the proton according to the formula

$$F_2^{em}(x, Q^2) = x \sum_i e_i^2 [q_i(x, Q^2) + \bar{q}_i(x, Q^2)]$$

where q_i indicates the probability density of finding a quark of flavour i and momentum fraction x in the proton (quark density function) at the virtuality scale Q^2 , e_i is the quark electric charge, and the sum runs over all flavours. For weak boson exchange the charge coefficients have to be adjusted accordingly, and mass as well as electroweak interference effects have to be taken into account.

Including first order (Fig. 1) and higher order QCD corrections, and/or non-negligible quark masses, such as for heavy quarks, this simple relation gets spoiled. In general, a measurement of the structure functions is thus *not* a direct measurement of the quark densities any more. However, these QCD and mass corrections are calculable and can be unfolded, such that the quark densities can still be extracted. In addition, the gluon density can also be obtained from these corrections, e.g. from the boson-gluon fusion (BGF) contribution (Fig. 1), and from the QCD evolution of the quark densities (Fig. 2). The gluon and quark densities are generically referred to as parton density functions (PDFs). The measurement and extraction of such PDFs is necessary because, due to the smallness of the quark and gluon masses, they can not be obtained from QCD using perturbative methods, and nonperturbative results, e.g. from lattice QCD, are not yet precise enough to be useful.

Note that this leads to varying definitions of the variables x and Q^2 , depending on the context. In the context of the measurement of nucleon structure functions through electroweak scattering, x and Q^2 are always strictly defined according to the mathematical definitions in section 2.1. On the other hand, in the PDFs, x

refers to the momentum fraction of the nucleon carried by the parton in the infinite momentum frame, while Q^2 refers to any hard scale at which the parton densities are probed, which can be e.g. the virtuality of a quark or gluon in a purely hadronic interaction. The two definitions coincide only in the simplest form of Quark Parton Model scattering. This is a frequent source of confusion.

The structure function F_L reflects the (small) contribution from longitudinally polarized photons, and is strongly dependent upon the gluon density. It is only relevant at high y . For measurements not sensitive to the high y region, it can often be safely neglected. In regions where it cannot be neglected, one can define the so-called reduced cross section

$$\sigma_r(x, Q^2) = F_2(x, Q^2) - \frac{y^2}{1 + (1 - y)^2} F_L(x, Q^2)$$

which is the quantity actually measured in the experiment, while both F_2 and F_L are derived quantities. The first direct determination of F_L was one of the primary goals of the last months of HERA running. Since this is covered by a separate contribution [2] it will not be discussed further here.

The structure function $x F_3$ is sensitive to quark-antiquark asymmetries related to weak interactions. For neutral current (NC, γ/Z exchange) interactions it is therefore only relevant at high Q^2 , when electroweak interference effects become important. Again, this part and the related electroweak fits are covered by a separate contribution [3].

2.3 The structure function F_2

Fig. 3 shows a combination of all relevant measurements [4] of the reduced cross section (essentially F_2) as a function of x and Q^2 from HERA I results and fixed target experiments, together with a QCD-based parametrization. The positive slope with respect to Q^2 (so-called scaling violations) at low x is caused by the splitting of gluons into $q\bar{q}$ pairs, which becomes visible at high resolution (high Q^2), while the negative slope at high x is caused by gluon radiation from the high x valence quarks, reducing their effective energy/momentum when looked at with increasing resolution (Fig. 2).



Figure 2: Diagrams contributing to the PDF evolution in leading order QCD. Gluon splitting to quarks (left) and gluon radiation off a quark (right).

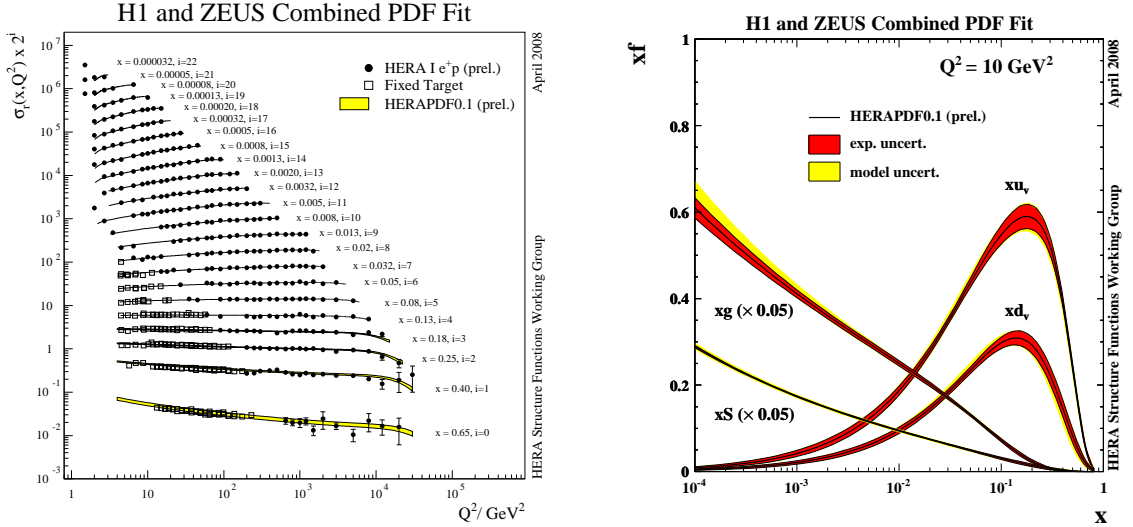


Figure 3: Left: The reduced cross section σ_r as a function of Q^2 for different values of x , compared to the HERAPDF0.1 fit [4]. For better visibility, offsets have been applied to each curve as indicated in the axis label. Right: The parton density functions (u and d valence quarks, sea quarks, and gluons) as a function of x at $Q^2 = 10 \text{ GeV}^2$. For better visibility, the sea and gluon distributions have been scaled down by a factor 20.

This so-called DGLAP parton evolution [5] is predicted by perturbative QCD and uniquely fixes the theoretical parametrization at any Q^2 once a parametrization at a given initial Q^2 is given. Combined with global energy and momentum conservation, this significantly constrains the gluon density function. In addition to a reduction of the statistical error, the combination of data points from ZEUS and H1 also leads to a reduction of the systematic error through the so-called cross-calibration effect [4].

Fig. 3 also shows a parametrization [4] of all these measurements in terms of the parton densities at the scale $Q^2 = 10 \text{ GeV}^2$. While the valence quark distributions (difference between quark and antiquark distributions) peak at high x values, the gluon and sea quark distributions rise strongly at low x , as expected from the DGLAP parton evolution. The data combination procedure mentioned above allows a very significant reduction of the experimental errors of the parton density extraction, reflected by the small uncertainty bands in Fig. 3. The model uncertainties within the ZM-VFNS scheme (see below), in which these PDFs have been extracted, are also indicated. Further improvements are expected on the experimental side from the inclusion of HERA II data, and on the theoretical side by including heavy quark mass effects.

Fig. 4 shows the kinematic range covered by experiments which contribute to the measurements of the parton densities. In addition to the lepton nucleon scattering

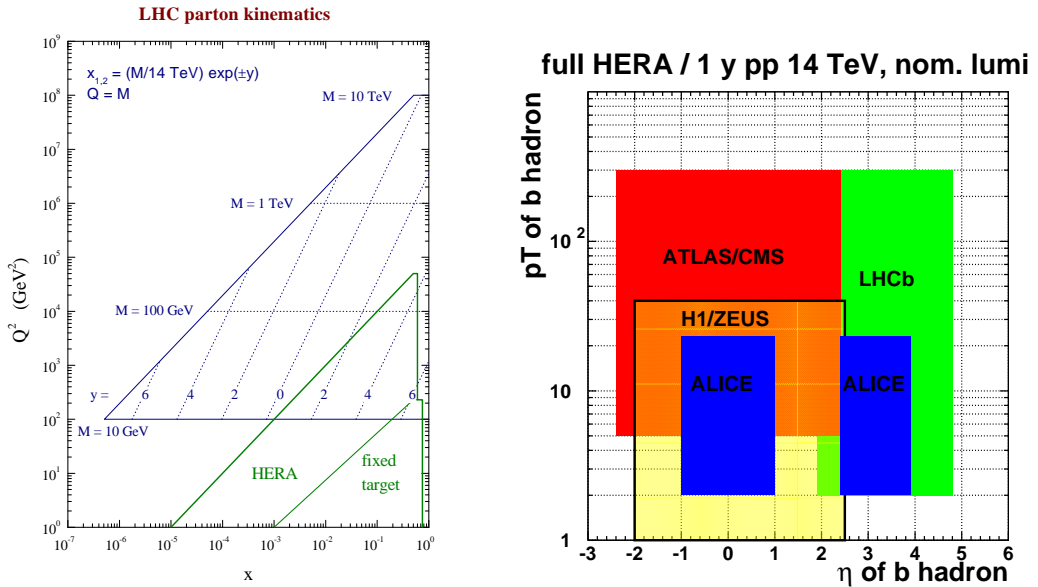


Figure 4: Left: Kinematic plane in x and Q^2 probed by HERA, fixed target experiments, and the LHC [6]. Right: kinematic acceptance for beauty production at LHC for 1 year of running at nominal luminosity [7] (boxes without boundary) compared to beauty production at HERA for the full final dataset (box with boundary).

experiments, measurements at the Tevatron $p\bar{p}$ collider also contribute at high Q^2 . The kinematic region relevant for measurements at the LHC is also shown, as a grid indicating the relevant mass and detector rapidity regions. Despite significant overlap between this region and the HERA+Tevatron measurements, a large fraction of the phase space is not covered by direct measurements at other colliders. It therefore has to be (and can be) extrapolated from the measurements at lower Q^2 through QCD parton evolution as explained above. On the other hand, there is also significant overlap in the kinematic coverage for the measurement of specific final states, as illustrated by the example of beauty production in Fig. 4.

Most cross sections at LHC depend on the square of either the quark or the gluon distributions. This illustrates the importance of a precise determination of these PDFs, both through direct measurements and through the detailed understanding of the QCD parton evolution, even at lower energies.

In the early 1980s, the PDFs determined and evolved at leading order (LO) from structure function measurements at fixed target energies [8] were used very successfully to predict the cross sections for W,Z and jets to be expected at the CERN Sp \bar{p} S collider. The current state of the art uses next-to-leading order (NLO) QCD evolution to predict the cross sections at LHC from the measurements at HERA (and the Tevatron), with first successful attempts to go beyond NLO accuracy.

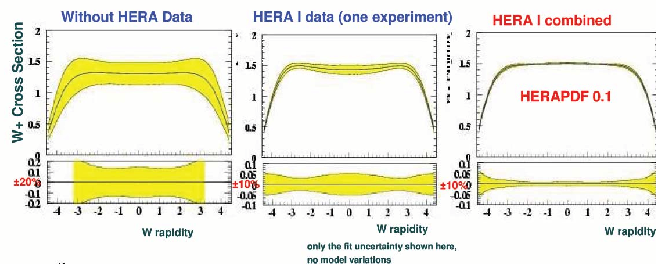


Figure 5: Predictions [9] for W production at LHC using fixed target data only (left) HERA I data from one of the two experiments (center) and the combined HERAPDF0.1. Only the experimental uncertainties are shown here for illustration.

Predictions for the production of W bosons at LHC without using HERA data, using the HERA I results from one experiment only, and using the HERAPDF0.1 (with experimental uncertainties only) are shown in Fig. 5. The improvement is obvious.

2.4 The heavy flavour contribution to F_2

In general, all quark flavours contribute to F_2 at all values of Q^2 and x . However, if m_Q is the mass of a heavy quark (charm or beauty), the 0^{th} order QPM process in Fig. 1 is kinematically allowed only for $Q^2 > (2m_Q)^2$ (“heavy quark threshold”), and its kinematics is strongly affected by the quark mass until $Q^2 \gg (2m_Q)^2$. In the latter case the mass becomes negligible, and the theory can be treated as if the heavy quarks were massless. A PDF can be defined for them like for the light quarks (zero mass variable flavour number scheme, ZM-VFNS). For $Q^2 \lesssim (2m_Q)^2$ a description is possible only in terms of 1^{st} or higher order QCD processes (e.g. the BGF process in Fig. 1), in which the heavy quarks are only produced perturbatively in the matrix element, with no heavy quarks in the PDFs. Since heavy flavour final states are always perturbatively calculable ($m_Q \gg \Lambda_{QCD}$) this so-called fixed flavour number scheme (FFNS) can be analytically continued to the full phase space as an alternative description valid at all¹ Q^2 . In particular, the FFNS approach works down to $Q^2 \rightarrow 0 \text{ GeV}^2$, i.e. the photoproduction regime. Of course, the formal values of Q^2 and x in F_2 become meaningless in this context, and have to be replaced by suitably chosen other kinematic variables. Finally, finite mass effects can be introduced as corrections to the ZM-VFNS scheme at medium Q^2 , and smoothly matched to a pure FFNS treatment at low Q^2 . This so-called general mass variable flavour number scheme (GM-VFNS) is an alternative to the FFNS scheme valid at all $Q^2 \gtrsim 1 \text{ GeV}^2$.

¹It is frequently claimed that the FFNS scheme will stop being valid at high Q^2 due to the occurrence of corrections of the type $\log(Q^2/m_Q^2)$. This is correct in principle. However, within most of the kinematic range of HERA, such logs turn out not to be numerically very important.

However, in higher order corrections, the mass treatment differs in different variants of this scheme [10].

At high Q^2 , charm and beauty quark densities can then be extracted in analogy to light quarks, and be applied to other high energy processes such as $b\bar{b} \rightarrow Z, H$ production at LHC. This contribution to the Z final state is relevant for the absolute luminosity measurement at LHC, while the Higgs (H) boson final state represents an obvious interest by itself.

Heavy flavours such as charm and beauty thus need some special treatment for the interpretation of F_2 in terms of PDFs, and it is interesting to measure their contribution separately. In order to determine the primary quark flavour which has participated in the interaction, this flavour has to be tagged and identified. In contrast to inclusive F_2 measurements, it is thus necessary to measure details of the hadronic final state. The contributions to F_2 which contain a pair of charm or beauty quarks in the final state are often denoted by $F_2^{c\bar{c}}$ and $F_2^{b\bar{b}}$, respectively. A summary of measurements of these contributions are shown in Fig. 6.

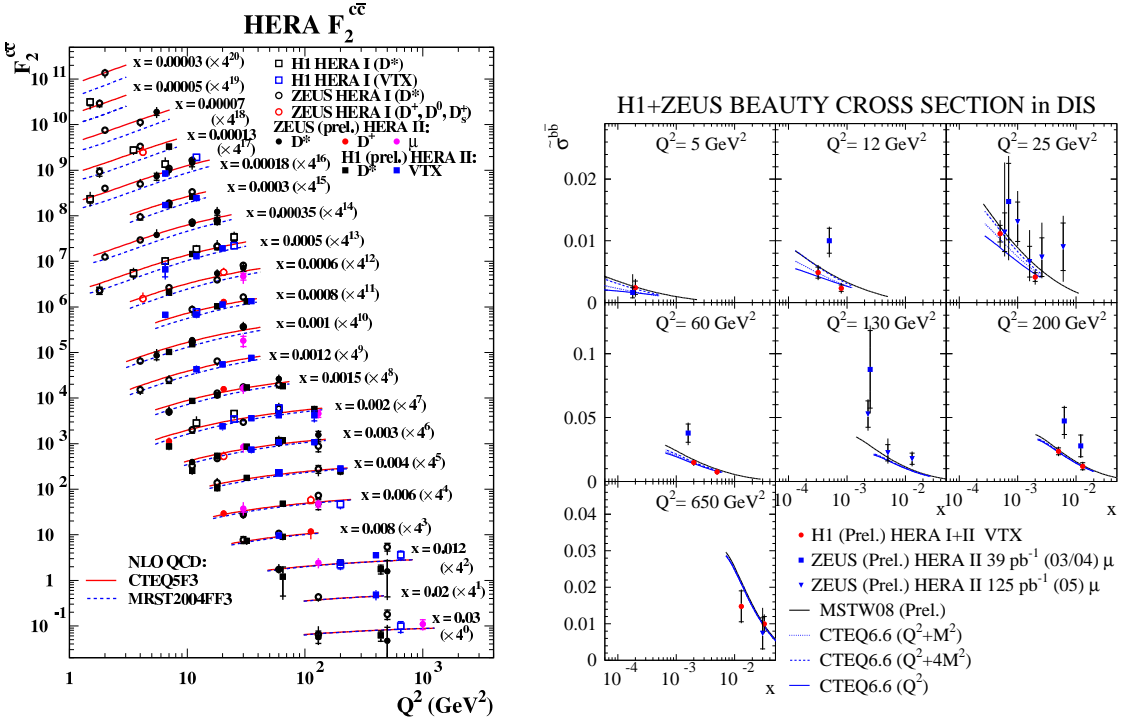


Figure 6: Left: The charm contribution to the proton structure function, $F_2^{c\bar{c}}$, as a function of Q^2 for different values of x , compared to two FFNS predictions. For better visibility, offsets have been applied to each curve as indicated on the plots. Right: The reduced cross section for the beauty contribution to the proton structure function, $\tilde{\sigma}^{b\bar{b}}$, as a function of Q^2 for different values of x , compared to different GM-VFNS predictions.

Below and around the QPM “threshold” at $Q^2 \sim (2m_Q)^2$, an interpretation of $F_2^{Q\bar{Q}}$ ($Q = c, b$) in terms of quark density functions is not possible. Instead, its interpretation in terms of QCD contributions like the BGF diagram in Fig. 1 can be used to verify the gluon density.

As can be seen from Fig. 6 the spread of the theory predictions due to the choice of scheme, QCD reference scale, value of the heavy quark mass, and other effects is still quite large. While the precision of the data will increase further (so far, only a fraction of the available data has been analyzed) these uncertainties will have to be reduced in order to allow a high precision determination of e.g. the gluon density from these data.

In summary, in view of the increasing precision of the data, no single theoretical scheme has been identified so far which simultaneously and fully satisfactorily treats all aspects of the (at least) three different QCD scales Q^2 , m_Q , and p_T at NLO or beyond. This is known as the multiple hard scale problem. While this often leads to complications for the prediction of heavy-flavour-related cross sections, its effect on the predictability of inclusive cross sections (which contain heavy flavours) is fortunately much smaller, but not negligible.

3 Global QCD fits and the strong coupling constant

The possibility to test or constrain the gluon distribution through the measurement of heavy flavours, e.g. from boson gluon fusion, was already addressed in the previous section. In a similar way, light quark cross sections can also be used in both DIS and photoproduction if another hard scale is present, such as a high transverse momentum (p_T) of the quarks, manifesting itself through the occurrence of high p_T jets in the final state.

Since jet production is also sensitive to the value of α_s (NLO calculations are available), a global simultaneous QCD fit to both F_2 and jet cross sections [11] can be made, so far to ZEUS data only. This indeed yields an improved gluon PDF (Fig. 7) as well as one of the currently best measurements of α_s ,

$$\alpha_s(M_Z) = 0.1183 \pm 0.0028(\text{exp.}) \pm 0.0008(\text{model}) \pm 0.0050(\text{th.})$$

where the first error contains the experimental errors, the second refers to model uncertainties in the α_s extraction, and the third reflects the usual scale variations of the NLO QCD predictions. Like in most α_s measurements to NLO, the theoretical uncertainties unfortunately dominate.

Global fits also including charged current data and electroweak effects, which can yield further improvements, are treated elsewhere [3].

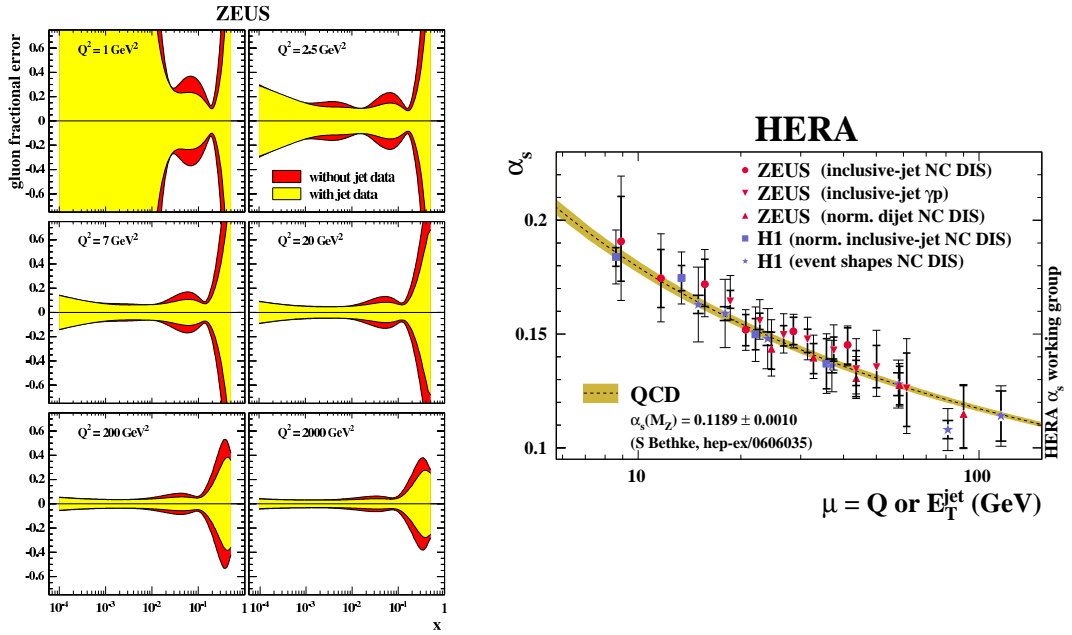


Figure 7: Left: The gluon density from ZEUS data as a function of x at different values of Q^2 , with and without the inclusion of jet data into the fit. A significant improvement can be seen. Right: Determinations of α_s at HERA from many different final states. The running of α_s is clearly visible.

Alternative determinations of the strong coupling constant α_s can be obtained from many dedicated measurements at HERA (Fig. 7). A subset of these measurements, selected to minimize the theoretical uncertainties, has been used for a first combined measurement from both ZEUS and H1 data. The resulting value

$$\alpha_s(M_Z) = 0.1193 \pm 0.0019(\text{exp.}) \pm 0.0026(\text{th.})$$

has an experimental error which is significantly smaller than each of the input measurements, but is still dominated by the theoretical uncertainty.

A recent measurement of H1 [15], aiming at a minimization of the experimental uncertainties, has obtained a value

$$\alpha_s(M_Z) = 0.1193 \pm 0.0014(\text{exp.})^{+0.0047}_{-0.0030}(\text{th.}) \pm 0.0016(\text{pdf}).$$

Combining such results between H1 and ZEUS, and integrating them into global fits, is expected to further reduce the experimental uncertainties. The goal to reduce the theoretical uncertainties through NNLO calculations should thus be of utmost priority. Once available, they will allow the worlds most precise determinations of the strong coupling constant. If supersymmetry is discovered at LHC, this could e.g. be decisive to determine whether the three Standard Model coupling constants can

be merged into a single one at some very high scale in the context of supersymmetric Grand Unified Theories.

4 Parton dynamics at low x

From Fig. 4 it is evident that the very low x region is particularly relevant for LHC. Since no direct measurements exist in this region, parton evolution from high to low x and/or low to high Q^2 is needed. A study of the low x region at HERA reveals that such an evolution is not trivial.

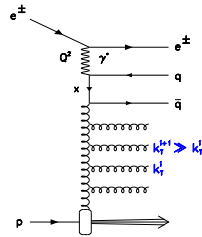


Figure 8: Feynman graph for multijet production at HERA involving an initial state gluon ladder.

Fig. 8 shows the example of a Feynman graph involving multiple initial state gluon radiation (gluon ladder). At HERA, such gluons can lead to detectable jets in the forward (proton) direction [12]. From the theoretical point of view, they can be treated as part of the matrix elements, which then have to be calculated to a very high order, which is difficult in practice. Alternatively, they can be treated as parton showers, using different evolution schemes. In the standard DGLAP [5] scheme, gluon emissions are ordered by increasing virtuality (k_T -ordering). In the alternative BFKL [13] scheme ordering in x is used instead. The two schemes can be combined into the CCFM [14] scheme which uses angular ordering. Forward jet measurements in 4-jet final states at HERA [12] show that the leading order matrix element plus next-to-leading log DGLAP parton shower approach partially fails. The NLO ($O(\alpha_s^2)$, effectively "LO") plus collinear DGLAP evolution scheme also fails in some cases. Going to NNLO ($O(\alpha_s^3)$, effectively "NLO") starts to yield a reasonable but, in the case of H1, still not perfect description. An NNNLO calculation might be needed within the DGLAP approach. Unfortunately a corresponding prediction using BFKL evolution is not yet available. However, the prediction from the color dipole parton showering model, using $k-T$ unordered gluons like BFKL, yields a very good agreement. This might indicate that a BFKL-like evolution can be of advantage in the low x region. Further studies and measurements are needed to quantify the consequences for cross section predictions at the LHC.

More details on this topic can be found in [1].

5 Photons and heavy flavours in photoproduction

Further insights into the validity of perturbative QCD can be obtained from the photoproduction of final states including direct photons or heavy flavours. As an example, a summary of measurements of the beauty production cross section is shown in Fig. 9. Reasonable agreement is observed over the full kinematic range. This enhances the confidence in corresponding QCD calculations for the LHC.

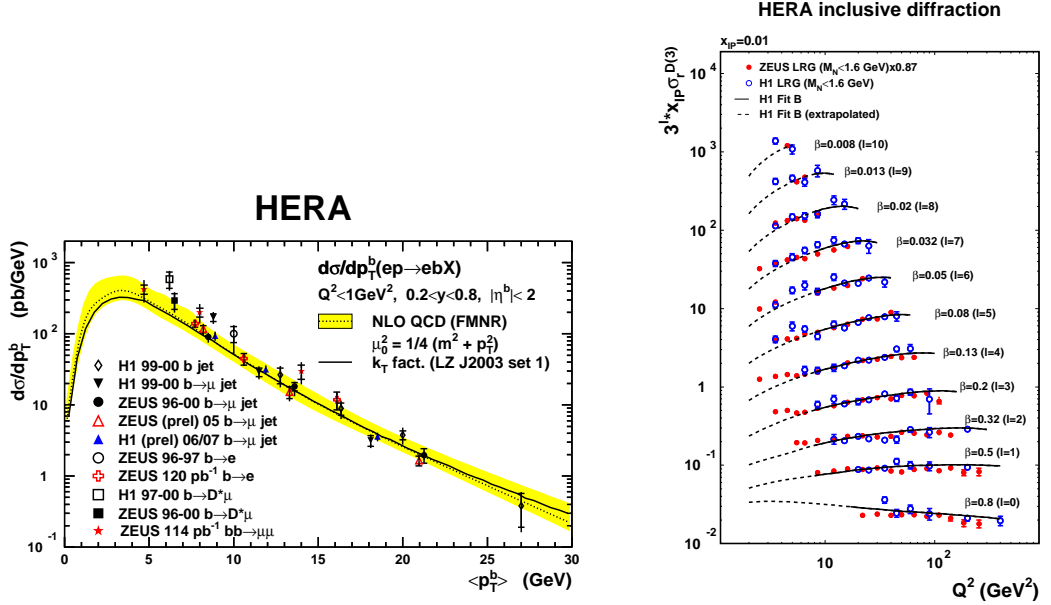


Figure 9: Left: Beauty production cross section at HERA as a function of p_{Tb} . QCD predictions from an NLO fixed order calculation [16], and from a calculation using the CCFM approach (k_T fact.) [17] are also shown. Right: Reduced cross section for inclusive diffractive final states in deep inelastic scattering at HERA [18]. The ZEUS data are scaled by a factor compatible with the relative normalization uncertainty of the two experiments. The continuous lines are the prediction from a QCD fit of part of these data. The dashed lines indicate predictions outside of the validity region of the fit.

6 Diffraction

Diffractive production (i.e. via the exchange of a colourless hadronic state with vacuum quantum numbers, sometimes called a pomeron) of vector mesons and/or inclusive hadronic final states yields another handle to study nonperturbative QCD

effects and their perturbative evolution at high scales, assuming factorization. A so-called diffractive structure function can then be defined, to be understood as the fraction of the proton structure function yielding diffractive final states.

Diffractive production of vector mesons at HERA is covered in [19]. Inclusive diffraction can be studied in three different ways:

- The detection of a large rapidity gap in the hadronic final state, caused by the colorless exchange.
- The measurement of the mass distribution of the detected hadronic final state (M_X method).
- Explicit detection of a scattered unbroken proton.

Fig. 9 shows a comparison of the diffractive structure functions measured by ZEUS and H1 using the large rapidity gap method on deep inelastic scattering events. Reasonable agreement is observed. The resulting PDFs can then be used to predict other cross sections at HERA, as well as at the Tevatron and the LHC. Many of these cross sections can currently only be explained by introducing a semi-empirical rapidity gap survival (or suppression) factor. Understanding the QCD origin of this suppression is currently one of the most topical aspects of diffraction, with direct consequences e.g. for the prediction of diffractive Higgs production at the LHC.

7 Conclusions

HERA is currently one of the best QCD laboratories. Measurements at HERA (at the “HERAscale”) are generally in good agreement with predictions from perturbative QCD calculations, which represents a great success of the Standard Model. They also provide valuable information for measurements at the LHC (the Terascale), such as precise parametrisations of the parton density functions, precise determinations of the strong coupling constant, and insights into the treatment of QCD at low x , the treatment of finite quark masses, and the treatment of diffractive processes. In many cases, the most precise final results with the full HERA statistics are still to come.

References

- [1] C. Royon, these proceedings
- [2] V. Chekelian, these proceedings
- [3] E. Gallo, these proceedings

- [4] H1 and ZEUS collaborations, *QCD fits using combined H1 and ZEUS inclusive data*, H1prelim-08-045, ZEUS-prel- 08-003 (2008).
- [5] V.N. Gribov and L.N. Lipatov, *Sov. J. Nucl. Phys.* **15** (1972) 438;
L. N. Lipatov, *Sov. J. Nucl. Phys.* **20** (1975) 95;
G. Altarelli and G. Parisi, *Nucl. Phys.* **B 126** (1977) 298;
Yu.L. Dokshitzer, *Sov. Phys. JETP* **46** (1977) 641.
- [6] W.J. Stirling, CAVENDISH-HEP-08-15, arXiv:0812.2341, dec. 2008.
- [7] A. Dainese et al., *Proceedings of HERA and the LHC*, p. 357, A. de Roeck and H. Jung (eds.), CERN-2005-014, dec. 2005.
- [8] see e.g. E. Eichten et al., *Rev. Mod. Phys.* **56** (1984) 579; **58** (1986) 1065.
- [9] A. Cooper-Sarkar, private communication
- [10] R. Thorne and W.K. Tung, *Proceedings of HERA and the LHC* (to be published), arXiv:0809.0714 [hep-ph].
- [11] ZEUS collaboration, S. Chekanov et al., *Eur. Phys. J. C* **42** (2005) 1.
- [12] H1 Collaboration, A. Aktas et al., *Eur. Phys. J. C* **48** (2006) 715.
ZEUS Collaboration, S. Chekanov et al., *Nucl. Phys.* **B 786** (2007) 152.
- [13] E.A. Kuraev, L.N. Lipatov, and F.S. Fadin, *Phys. Lett.* **B 60** (1975) 50; *Sov. Phys. JETP* **44** (1976) 443; *Sov. Phys. JETP* **45** (1977) 199;
Ya.Ya. Balitsky and L.N. Lipatov, *Sov. J. Nucl. Phys.* **28** (1978) 822.
- [14] M. Ciafaloni, *Nucl. Phys.* **B 296** (1988) 49;
S. Catani, F. Fiorani and G. Marchesini, *Phys. Lett.* **B 234** (1990) 339; *Nucl. Phys.* **B 336** (1990) 18;
G. Marchesini, *Nucl. Phys.* **B 445** (1995) 49.
- [15] H1 Collaboration, A. Aktas et al., *Phys. Lett.* **B 653** (2007) 134.
- [16] S. Frixione, M. L. Mangano, P. Nason and G. Ridolfi, *Nucl. Phys.* **B 412** (1994) 225; *Phys. Lett.* **B 348**, 633 (1995);
S. Frixione, P. Nason and G. Ridolfi, *Nucl. Phys.* **B 454** (1995) 3.
- [17] A.V. Lipatov, N.P. Zotov *Phys. Rev.* **D 73** (2006) 114018.
- [18] M. Ruspa, in *Proceedings of HERA and the LHC* (to be published).
- [19] W. Bartel, these proceedings.